

# Obtaining high-precision predictions for jet production at the LHC in perturbative QCD

Hugo Amaral<sup>1, a</sup>

<sup>1</sup>Instituto Superior Técnico, Lisboa, Portugal

Project supervisor: J. Pires

October 13, 2023

**Abstract.** In this project we study perturbative Quantum Chromodynamics with the purpose of obtaining high-precision prediction for jet production at the LHC. We began by using RAMBO phase space generator to generate 100 random events with 6 final state particles and an inclusive  $k_T$  algorithm was written using Matlab<sup>®</sup> to sort these into jets. Subsequently, using recent parton distribution function sets, LHAPDF[1] and the fastnlo[2, 3] libraries were used to obtain predictions in QCD for inclusive jet production for proton-proton collisions at  $\sqrt{s} = 7 TeV$ , the predictions were then compared to data from the ATLAS experiment. This study found no indication or evidence of new physics beyond the Standard Model for the single-jet inclusive observables studied at the LHC.

KEYWORDS: LHC, ATLAS, QCD, Jet Production, Fastnlo, LHAPDF

## 1 Introduction

### 1.1 The Standard model

The Standard model of particle physics embodies the current understanding of this field of physics. The Standard model postulates that the fundamental particles, and the corresponding anti-particles, are classified into four groups: the Leptons, Quarks, Gauge bosons and the Higgs boson, and that the fundamental forces are described as the interactions of the fundamental particles through the exchange of a particle in the Gauge boson group [4]. The Electromagnetic force is mediated by the exchange of a photon and is described by the theory of Quantum Electrodynamics (QED), the strong force is mediated by the exchange of a gluon and is described by the theory of Quantum Chromodynamics (QCD) the weak force is mediated by the exchange of a charged  $W^\pm$  boson or a neutral  $Z^0$  boson. Figure 1 shows a table of the fundamental particles in the Standard model, with some of their properties.

	mass → ≈2.3 MeV/c <sup>2</sup>	≈1.275 GeV/c <sup>2</sup>	≈173.07 GeV/c <sup>2</sup>	0	≈126 GeV/c <sup>2</sup>
	charge → 2/3	2/3	2/3	0	0
	spin → 1/2	1/2	1/2	1	0
	<b>u</b>	<b>c</b>	<b>t</b>	<b>g</b>	<b>H</b>
	up	charm	top	gluon	Higgs boson
QUARKS	≈4.8 MeV/c <sup>2</sup>	≈95 MeV/c <sup>2</sup>	≈4.18 GeV/c <sup>2</sup>	0	
	-1/3	-1/3	-1/3	0	
	1/2	1/2	1/2	1	
	<b>d</b>	<b>s</b>	<b>b</b>	<b>γ</b>	
	down	strange	bottom	photon	
LEPTONS	0.511 MeV/c <sup>2</sup>	105.7 MeV/c <sup>2</sup>	1.777 GeV/c <sup>2</sup>	91.2 GeV/c <sup>2</sup>	
	-1	-1	-1	0	
	1/2	1/2	1/2	1	
	<b>e</b>	<b>μ</b>	<b>τ</b>	<b>Z</b>	
	electron	muon	tau	Z boson	
GAUGE BOSONS	<2.2 eV/c <sup>2</sup>	<0.17 MeV/c <sup>2</sup>	<15.5 MeV/c <sup>2</sup>	80.4 GeV/c <sup>2</sup>	
	0	1/2	1/2	±1	
	1/2	1/2	1/2	1	
	<b>ν<sub>e</sub></b>	<b>ν<sub>μ</sub></b>	<b>ν<sub>τ</sub></b>	<b>W</b>	
	electron neutrino	muon neutrino	tau neutrino	W boson	

**Figure 1.** An image illustrating the Standard model of particle physics

<sup>a</sup>e-mail: hugo.amaral@tecnico.ulisboa.pt

### 1.2 Collisions at the LHC

At the LHC protons are grouped into bunches that are accelerated and made to collide at interaction points, where the detectors are located [4]. When two protons collide at high energies, the fundamental particles that form the proton interact with each other, these interactions are described by Feynman diagrams in section 3. The proton is composed of particles that have colour charge, Quarks and gluons, and interact with each other through the strong force, and so the particles resulting from the collisions can have color charge and emit QCD radiation through Bremsstrahlung. However, because of colour confinement, a not fully understood property of QCD that dictates that a particle with colour charge cannot exist in a free-particle state, the resulting particles go through the process of hadronization. Final state QCD radiation and hadronization is the process by which highly energetic colour charged particles produce hadrons in a collimated beam called a jet.

## 2 Jet Algorithm

In a proton-proton collision the experiments detect several hadrons resulting from the interaction between the fundamental partons of the protons, so, to study these events, it is necessary to group the particles into jets, and for this reason, the use of a jet-algorithm must be employed. In this section properties of a jet algorithm are established .

### 2.1 Main variables

Here we present a list of the variables that will be used by the jet algorithm to detect jets

- $\phi = \arctan \frac{P_x}{P_y}$  : azimuthal angle of the trajectory of a particle;
- $y = \frac{1}{2} \ln \left( \frac{E+P_z}{E-P_z} \right)$  : rapidity;
- $P_t = \sqrt{P_x^2 + P_y^2}$  : transverse momentum;

- $R$  : A parameter chosen to fix the size of the jet in the algorithm ;

## 2.2 Infrared and collinear safety

Infrared and collinear (IRC) safety is the property that if a soft or collinear particle is added to an event, the set of detected jets should remain unchanged [5]. An illustration of IRC unsafe effects on the detection of jets is shown in Figure 2

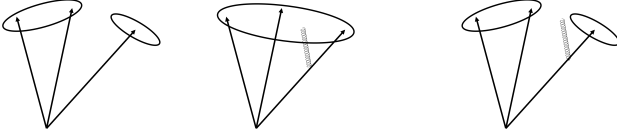


**Figure 2.** a) Configuration of two jets to demonstrate IRC safety, where b) shows an IRC unsafe algorithm and c) show an IRC safe algorithm

IRC safety is an important property of jet algorithms and must be accounted for, since:

- soft or collinear particle emissions occur randomly and their average properties involve non-perturbative effects making them harder to predict.
- In fixed-order perturbative QCD calculations soft and collinear emissions are associated with divergent tree-level matrix elements, there are also divergent loop matrix elements that have opposite sign. Normally these will cancel each other, but an IRC unsafe algorithm the tree-level divergences may lead to one set of jets and the loop diagram may lead to another set of jets creating infinite cross sections.
- Experimental detectors provide some regularisation of IRC unsafety due to their finite resolution and non-zero momentum thresholds, but this depends on the particular combination of tracking, electromagnetic calorimetry and hadronic calorimetry that is used by the experiment. This can make it difficult to connect experimental results for IRC unsafe algorithms to the predictions at hadron-level.

## 2.3 Anti- $k_T$ algorithm

In this section we describe the jet algorithm [5] that we implemented in our study. We begin by assigning the following distance measures between outgoing particles and between an outgoing particle and the beam,

$$d_{ij} = \min(P_{ii}^{2p}, P_{ij}^{2p}) \frac{\Delta R_{ij}^2}{R^2}, \quad \Delta R_{ij}^2 = (y_i - y_j)^2 + (\phi_i - \phi_j)^2$$

$$d_{iB} = P_{ii}^{2p},$$

Where  $p$  is a parameter to distinguish three different algorithms, when  $p = 1$  it is called the inclusive  $k_T$  algorithm, when  $p = 0$  it is called the Cambridge/Aachen algorithm, when  $p = -1$  it is called the anti- $k_T$ , independently of the value of  $p$  the algorithm goes as follows:

1. compute  $d_{ij}$  and  $d_{iB}$  for all particles and particles-pairs in the event.
2. find the minimum of  $d_{ij}$  and  $d_{iB}$ .
3. if  $d_{ij}$  is the minimum recombine the  $i$  and  $j$  particles into a new particle and return to step 1.
4. if  $d_{iB}$  is the minimum declare  $i$  to be a jet and remove it from the list of detections
5. restart the algorithm until no particle remains.

## 2.4 Algorithm implementation

Using the phase space generator RAMBO, 100 random events with 6 final state particles were generated and processed with the anti- $k_T$  jet algorithm implemented using Matlab®. In Figure 3 we show the distribution of the number of observed jets as a function of the jet radius parameter  $R$ . We observe that as we increase  $R$  more final-state particles are grouped together increasing the number of events with fewer jets. Conversely for small enough  $R$  each final state particle will form a separate jet thus increasing the number of observed jets in the final state.

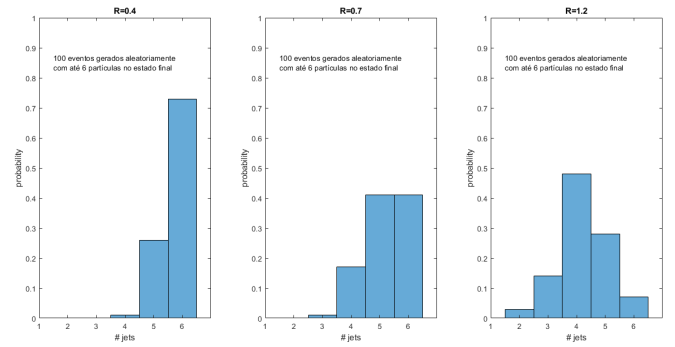


**Figure 3.** Histogram of the number of detected jets on an event using a)  $R = 0.4$ , b)  $R = 0.7$ , c)  $R = 1.2$

## 3 Feynman Diagrams for dijet production at leading order

In proton-proton collisions the partons of the protons interact with each other, which lead to the production of jets, for this project it is important to study the interactions that result in the production of two jets, through the use of Feynman diagrams. Table 1 shows all possible interactions between the constituents of the proton where  $g$ , is a gluon,  $q$  and  $\bar{q}$ , are the quark and anti-quark, respectively, and primed quarks and anti-quarks are used to show interactions between quarks and anti-quarks with different flavors.

Possible processes
$gg \rightarrow gg$
$gg \rightarrow q\bar{q}$
$qq' \rightarrow qq'$
$qq \rightarrow qq$
$qg \rightarrow qg$
$q\bar{q} \rightarrow q\bar{q}$
$q\bar{q}' \rightarrow q\bar{q}'$
$q\bar{q} \rightarrow gg$

**Table 1.** Possible processes for the interactions of the protons constituents

Some processes in Table 1 are related to each other by switching particles in the final state to the initial state in the transition matrix element, so we will only show some of the relevant leading-order Feynman diagrams. However, because of the different Parton Distribution Functions involved, all these processes must be summed.

$gg \rightarrow gg$

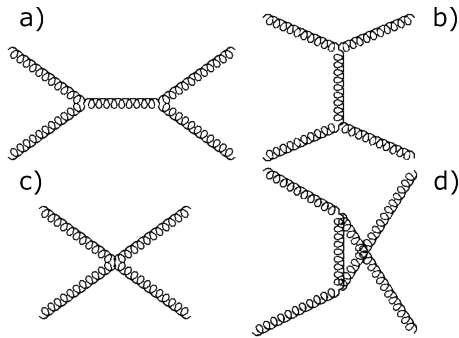


**Figure 4.** a) s-channel, b) t-channel, c) quartic gluon vertex, d) u-channel, according to the momenta carried by the propagator particle  $s = (p1 + p2)^2$ ,  $t = (p1 - p3)^2$ ,  $u = (p1 - p4)^2$ .

$qq' \rightarrow qq'$

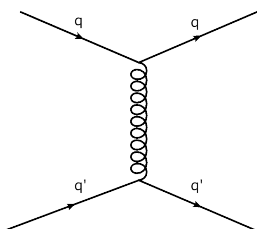


**Figure 5.** t-channel, according to the momenta carried by the propagator particle,  $t = (p1 - p3)^2$

$qq \rightarrow qq$

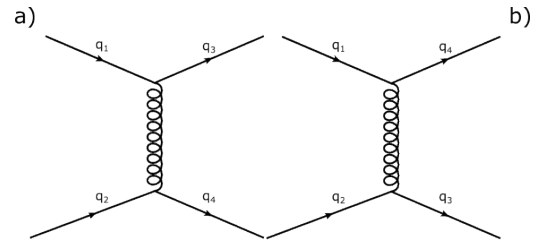


**Figure 6.** a) t-channel, b) u-channel, according to the momenta carried by the propagator particle,  $t = (p1 - p3)^2$ ,  $u = (p1 - p4)^2$

$q\bar{q} \rightarrow gg$

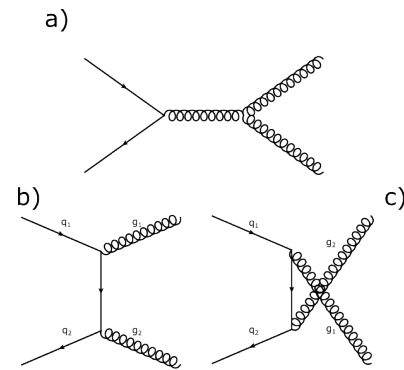


**Figure 7.** a) s-channel, b) t-channel, c) u-channel, according to the momenta carried by the propagator particle  $s = (p1 + p2)^2$ ,  $t = (p1 - p3)^2$ ,  $u = (p1 - p4)^2$

## 4 Parton Distribution functions

The fundamental particles within the proton interact with each other such that there exist a distribution of momenta within the constituents of the proton [4]. These distributions are expressed in *Parton distribution functions* (PDFs), however, because the strong force at the scale  $Q \approx 1 \text{ GeV}$  of the mass of the proton has a large coupling constant of  $\alpha \propto O(1)$ , perturbation theory cannot be used to calculate the PDFs from first principles. So the PDFs must be determined experimentally by fitting data from collider experiments and as an example, we show in Figure 8 a determination of the PDFs of the proton [6].

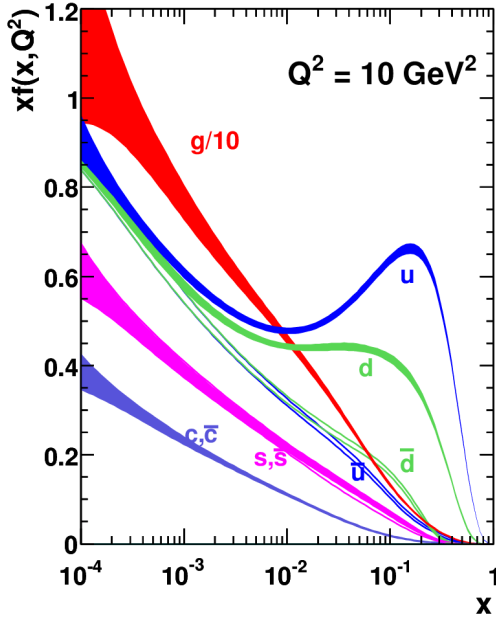


**Figure 8.** Proton PDFs for the quark, gluon and anti-quark densities at  $Q^2 = 10\text{GeV}^2$  as a function of the longitudinal momentum fraction  $x$  obtained by the MSTW 2008 collaboration, where the coloured bands represent the PDF uncertainty.

## 5 Results

In this work we used six different PDF sets which were evaluated using the LHADPF library to obtain predictions in perturbative QCD for the double differential in  $p_T$  and rapidity single jet inclusive cross section. To evaluate the perturbative component of the cross section we used, in addition, the FastNLO library [2, 3], which reads fast interpolation tables of pre-computed coefficients in perturbation theory up to Next-to-Next-to-Leading-Order (NNLO) in QCD for the single jet inclusive cross section. The double differential cross section for jet  $p_T$  in the range [100-2000] GeV and rapidity  $|y| \in [0 - 3]$  at NNLO in perturbative QCD is shown in Figure 9 for proton-proton collisions at  $\sqrt{s} = 7$  TeV using the anti- $k_T$  algorithm with  $R = 0.6$ . In the theory prediction we fixed the renormalization and factorization scale to the  $p_T$  of the reconstructed jet.

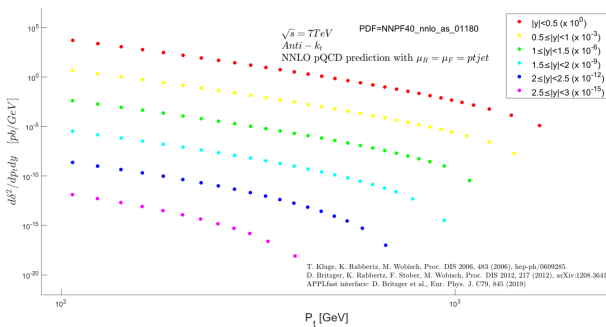


**Figure 9.** Double differential single jet inclusive cross section as a function of  $p_T$ .

The ratio between the differential cross-section of for several PDF sets and the NNPDF40\_nnlo PDF at different rapidities,  $|y| \in [0 - 3]$ , is shown in Figure 10.

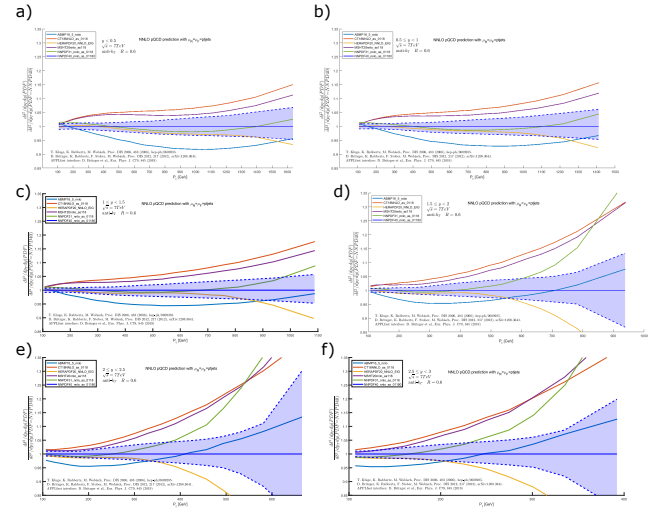


**Figure 10.** The ratio of the differential cross-section for a set of PDFs to the differential cross-section of PDF NNPDF40\_nnlo for a)  $|y| < 0.5$ , b)  $0.5 \leq |y| < 1$ , c)  $1 \leq |y| < 1.5$ , d)  $1.5 \leq |y| < 2$ , e)  $2 \leq |y| < 2.5$ , f)  $2.5 \leq |y| < 3$ , where the blue band shows the NNPDF40 PDF uncertainty at NNLO determined by the 100 replicas of this PDF set.

From Figure 10 we conclude that at low rapidities the PDF uncertainty is around 5% and all PDFs are compatible with each other, not deviating much. As the jet rapidity increases, the PDF uncertainty increases to around 20-30% and the different PDFs start to diverge and become incompatible. The ratio between the differential cross-section using Leading-Order (LO), Next-to-Leading-Order (NLO) and NNLO perturbative QCD predictions, which correspond to an increase in the perturbative order, with the NNPDF40\_nnlo PDF and the ATLAS data at different rapidities is shown in Figure 11 in green, blue and red respectively, with the respective uncertainty bands obtained by computing the predictions with  $\mu_R = \mu_F = 0.5 p_T$  and  $\mu_R = \mu_F = 2 p_T$ . In addition, there exists a contribution at the LHC at low-jet  $P_T$  from underlying event effects from the disintegration of the proton and from hadronization, which are non-perturbative corrections, and at high-transverse momenta the electroweak interactions has a noticeable effect and must be accounted for. We also plot in Figure 12 the perturbative QCD NNLO prediction reweighted for both these effects in magenta.

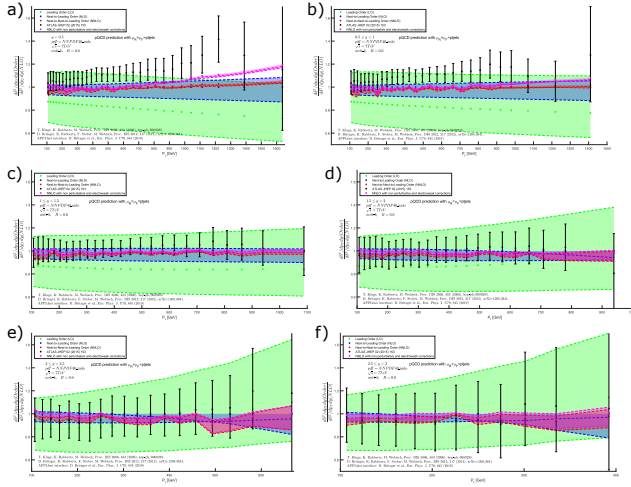


**Figure 11.** Ratio of differential cross-section for NNPDF40\_nnlo PDF using LO, NLO, NNLO and NNLO with non-perturbative and electroweak corrections and ATLAS data with uncertainty bands for a)  $|y| < 0.5$ , b)  $0.5 \leq |y| < 1$ , c)  $1 \leq |y| < 1.5$ , d)  $1.5 \leq |y| < 2$ , e)  $2 \leq |y| < 2.5$ , f)  $2.5 \leq |y| < 3$

From Figure 11 we conclude that, as we increase the perturbative order of the QCD calculation, the precision of the prediction also increases, making NNLO the most precise prediction and by applying the electroweak and non-perturbative interactions the resulting prediction becomes a better description of the ATLAS data as it can be seen in Figure 11 a).

The ratio of NNLO predictions for differential cross-section for several PDFs and ATLAS data to the differential cross-section for the NNPDF40\_nnlo PDF for several rapidities,  $|y| \in [0 - 3]$  is illustrated in Figure 12.

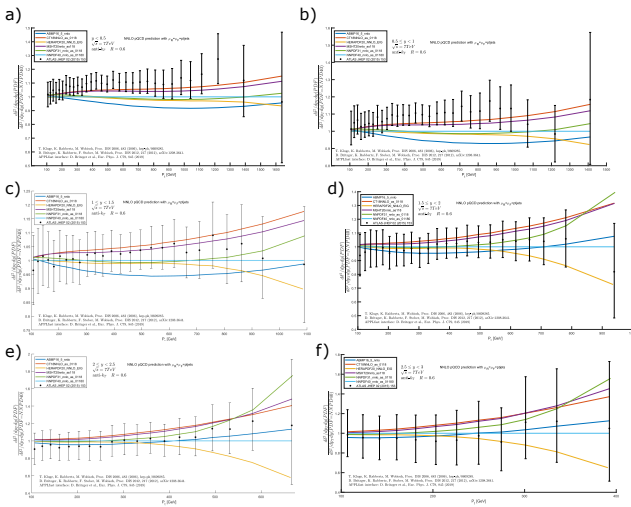


**Figure 12.** The ratio of the differential cross-section for the set of PDFs and ATLAS cross-section data to the differential cross-section of PDF NNPDF40\_nnlo for a)  $|y| < 0.5$ , b)  $0.5 \leq |y| < 1$ , c)  $1 \leq |y| < 1.5$ , d)  $1.5 \leq |y| < 2$ , e)  $2 \leq |y| < 2.5$ , f)  $2.5 \leq |y| < 3$

From Figure 12 we conclude that at low rapidities the CT18NNLO and MSHT20nnlo PDFs give the best de-

scription of the ATLAS experiment data, while at higher rapidities all PDFs are in good agreement within the larger uncertainty of the ATLAS data.

## 6 Conclusions

In this work, predictions for inclusive jet production cross section, differential in the jet transverse momentum and rapidity, using perturbative QCD up to NNLO in QCD, were obtained. It was concluded that different PDFs produce predictions of cross-section with a variation of 5% at low rapidity and 20-30% at high rapidity.

Comparatively, the perturbative accuracy at Next-to-Next-to-Leading-Order in QCD is at the level of 5% at low rapidity and less than 10% at high-rapidity as demonstrated by the width of the scale uncertainty bands in Figure 11.

Comparing theoretical predictions to experimental ATLAS data, the PDFs CT18 and MSHT20 were concluded to give the best description of the experimental data at low rapidity, while for high rapidities, all PDFs are compatible within the experimental uncertainties. This work concluded that there is no evidence for new physics in the measurement of the single jet inclusive cross section studied at the LHC.

## Acknowledgements

I would like to thank my supervisor, Doutor João Ramalho Pires, for allowing me to work on this project and for providing his guidance through this project. I would like to thank LIP and the LIP Summer Internship program for providing the opportunity and conditions that allowed the realization of this project.

## References

- [1] A. Buckley, J. Ferrando, S. Lloyd, K. Nordström, B. Page, M. Rüfenacht, M. Schönherr, G. Watt, *The European Physical Journal C* **75** (2015)
- [2] T. Kluge, K. Rabbertz, M. Wobisch, *fastNLO: Fast pQCD Calculations for PDF Fits*, in *Deep Inelastic Scattering DIS 2006* (2007), pp. 483–486, arXiv:hep-ph/0609285, <http://arxiv.org/abs/hep-ph/0609285>
- [3] D. Britzger, K. Rabbertz, F. Stober, M. Wobisch, *New features in version 2 of the fastNLO project* (2012), arXiv:1208.3641 [hep-ph], <http://arxiv.org/abs/1208.3641>
- [4] M. Thomson, *Modern particle physics* (Cambridge University Press, Cambridge, United Kingdom ; New York, 2013), ISBN 978-1-107-03426-6
- [5] G.P. Salam, *The European Physical Journal C* **67**, 637 (2010), arXiv:0906.1833 [hep-ph]
- [6] A.D. Martin, W.J. Stirling, R.S. Thorne, G. Watt, *The European Physical Journal C* **63**, 189 (2009)